CHEMISTRY OF MATERIALS

ARTICLE

pubs.acs.org/cm

Mechanism of Self-catalytic Atomic Layer Deposition of Silicon Dioxide Using 3-Aminopropyl Triethoxysilane, Water, and Ozone

Vikrant R. Rai and Sumit Agarwal*

Department of Chemical Engineering, Colorado School of Mines, Golden, Colorado 80401, United States

Supporting Information

ABSTRACT: We have investigated the surface reaction mechanism during the atomic layer deposition (ALD) of SiO_2 from 3-aminopropyl triethoxysilane (APTES), H_2O, and O_3 using in situ attenuated total reflection Fourier-transform infrared spectroscopy. After the chemisorption of APTES on the SiO_2 surface, during the H_2O cycle, the aminopropyl groups in APTES catalyze the hydrolysis of ethoxy ligands, leaving the surface terminated with OH groups—a reaction that would otherwise require an acidic or basic catalyst. O_3, in the subsequent cycle, combusts the remaining aminopropyl ligands, possibly producing combustion products such as CO, CO_2, H_2O, and NO_x. Among these products CO reacts with surface OH groups to form monodentate formates and SiH on the surface. The formates and SiH groups produced during O_3 exposure along with the OH groups produced during H_2O exposure serve as the reactive sites for APTES chemisorption, thus completing the entire ALD cycle.

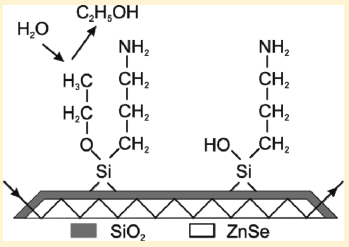

KEYWORDS: atomic layer deposition, aluminum oxide, ATR-FTIR spectroscopy, APTES, ozone

1. INTRODUCTION

SiO_2 is one of the most widely used dielectric materials in the microelectronics industry.[1] The excellent interface[1] between an ultrathin layer of SiO_2 and Si offers several advantages in CMOS devices, including improved nucleation of high-κ metal oxides and a reduced equivalent oxide thickness (EOT) of the SiO_2/high-κ bilayer.[2] Deposition of high-κ metal oxides, such as HfO_2, directly on H-terminated Si inadvertently leads to the formation of interfacial SiO_2, increasing the EOT.[3] An ultrathin (<0.5 nm) and conformal SiO_2 film deposited by atomic layer deposition (ALD)[4,5] can combine the advantages of the excellent Si/SiO_2 interface, improved nucleation, and a reduced EOT.[2] Furthermore, the ability to deposit high-quality, ultrathin, conformal SiO_2 films by ALD can widen its applications in dielectric nanolaminates for improved electrical properties,[6] optical coatings,[7] surface passivation layers for Si-based solar cells,[8] and coating of mechanical resonators in micro-/nanoelectromechanical systems to enable surface functionalization.[9]

Numerous thermal and plasma-assisted ALD processes have been developed for metal oxides. There are several studies of SiO_2 ALD as well reported in the literature, but it remains one of the most challenging materials to deposit via this process. Some of the common inorganic and organic Si sources used in the ALD of SiO_2 include $SiCl_4$,[10] SiH_2Cl_2,[11] $Si(N(CH_3)_2)_4$,[12] and $Si(NCO)_4$.[13] However, these precursors produce corrosive by-products such as HCl,[14] require long precursor exposure times at ≥300 °C,[11,13] and lead to residual C and/or N contamination.[12] Another self-limiting SiO_2 deposition method known as rapid ALD, which provides a growth per cycle of ~10−50 Å, utilizes tris(*tert*-butoxy)silanol[15] or tris(*tert*-pentoxy)silanol.[16] However, use of these precursors at low temperatures, ~25−150 °C, leads to C and OH impurities, and requires an additional metal catalyst.[15,16] Similarly, ALD of SiO_2 using tetraethoxy silane and H_2O has been reported by Ferguson et al., but requires NH_3 as a catalyst.[14] Recently, Bachmann et al. reported self-catalytic ALD of SiO_2 at 150 °C using 3-aminopropyl triethoxysilane (APTES), H_2O, and O_3 with C and N impurity levels <0.3 at. %.[17] However, the detailed surface reaction mechanism that leads to this self-catalytic growth has not been reported.

The underlying surface reactions during ALD play a very important role in film growth, and the gas-phase reaction products produced in each half-reaction cycle can strongly influence the growth process.[4] We have previously demonstrated this for O_3 and O_2 plasma-assisted ALD of TiO_2 and Al_2O_3 where the combustion products produced during the oxidation cycle led to the formation of carbonates on the surface,[18] which act as one of the reactive sites in the growth process.[19,20] In this article, we have elucidated the surface reactions during the ALD of SiO_2 from APTES in conjunction with sequential oxidation by H_2O and O_3 at 150 °C. The in situ attenuated total reflection Fourier transform infrared (ATR-FTIR) spectroscopy data are consistent with the hydrolysis of ethoxy ligands catalyzed by the NH_2 group in APTES during the H_2O cycle: this leads to the removal of ethoxy ligands as ethanol leaving the surface terminated by OH and aminopropyl groups. O_3, in the subsequent exposure, combusts the aminopropyl ligands, possibly producing CO, CO_2, H_2O, and NO_x, thus, depositing relatively contaminant-free films. The gas-phase species generated during the combustion-like reaction produces monodentate formates and silicon hydrides on the surface, which

Received: October 24, 2010
Revised: January 28, 2011
Published: April 15, 2011

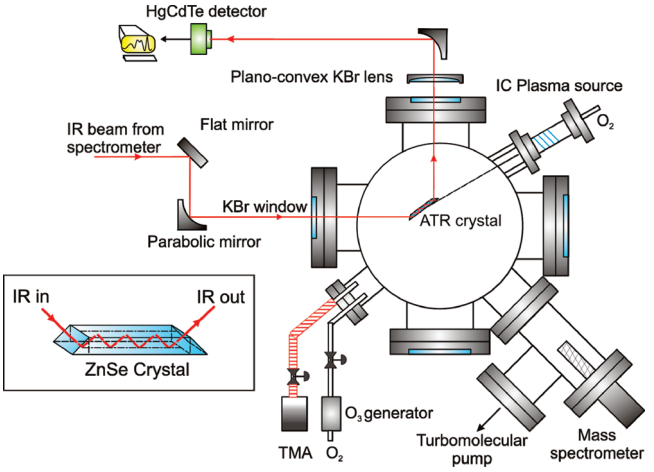

Figure 1. Schematic of the surface analysis chamber equipped with in situ ATR-FTIR spectroscopy. The red line shows the beam path for the He−Ne laser from the FTIR spectrometer through the IRE to the MCT-A detector.

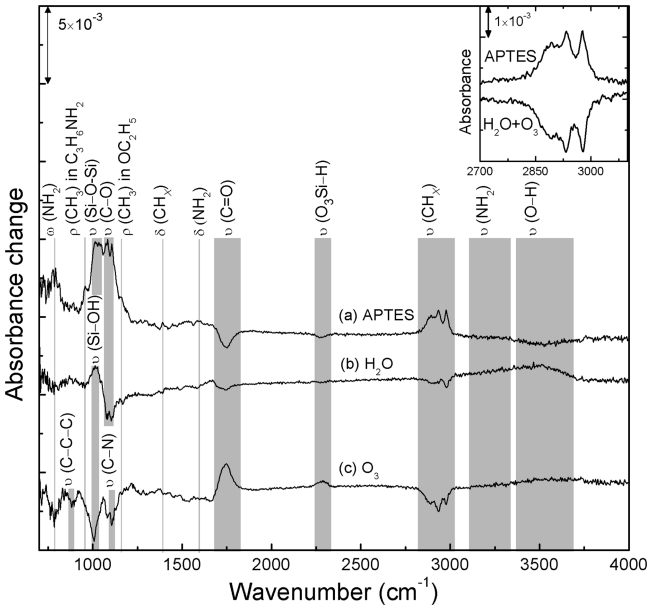

Figure 2. IR difference spectra recorded during APTES, H_2O, and O_3 reaction cycles at 150 °C. Vibrational modes for different surface species during the ligand-exchange reactions are indicated. Inset shows the CH_x ($x = 2, 3$) stretching region for APTES and combined H_2O and O_3 cycles.

are consumed in the subsequent APTES exposure. The presence of these additional reactive sites shows that the reaction sequence is more complex than what was speculated earlier by Bachman et al.[17]

2. EXPERIMENTAL SECTION

The surface chemistry during ALD of SiO_2 from APTES, H_2O, and O_3 was studied at 150 °C in a cold-wall vacuum chamber. The chamber was evacuated to a base pressure of ~10^{-3} Torr by a mechanical pump with a leak rate of ~0.5 mTorr/min. The chamber was equipped with a real-time in situ ATR-FTIR spectroscopy[21−25] setup. The schematic in Figure 1 depicts the top view of the main surface analysis chamber. In this setup, an infrared (IR) beam from an FTIR spectrometer (Nicolet 6700) was focused on to the beveled edge of a trapezoidal ZnSe internal reflection crystal (IRC) with dimensions of 1 mm ×10 mm ×50 mm, and the short faces polished at an angle of 45°. Since the angle of incidence of the IR beam on the flat face of the IRC was greater than the angle for total internal reflection, the IR beam was internally reflected 25 times on each flat face of the IRC before it emerged from the opposite beveled edge, and was directed to a liquid N_2-cooled mercury cadmium telluride (MCT-A) detector. All the optical components in the IR beam path were kept in a Plexiglas chamber constantly purged with CO_2-free dry air. Because of the refractive index mismatch between ZnSe (n ~2.4) and the ALD-deposited SiO_2 (n ~1.46), total internal reflection of the IR beam occurred at the film−crystal interface. The surface species were therefore probed by the evanescent field that decays exponentially into vacuum. This IR setup was also sensitive to the gas-phase species due to the ~20 cm long IR beam path through the chamber. The ZnSe IRC was clamped in a groove on a stainless steel substrate stage heated using two 100 W resistive cartridge heaters (Watlow Firerod). A K-type thermocouple was mounted directly behind the IRC, on the back face of the substrate stage, to measure the substrate temperature. The temperature was controlled within ±1 °C of the set point using a proportion-integral-derivative controller (Omega CN9000A).

APTES was delivered into the chamber through a bubbler maintained at 85 °C and 100 Torr. The delivery lines were heated to the same temperature to avoid any precursor condensation. N_2 was used as the carrier gas for APTES while Ar was used as the purge gas between each precursor exposure cycle. Deionized water was contained in a bubbler at 20 °C with the delivery line heated to ~90 °C to avoid condensation. An in-line corona-discharge-based O_3 generator supplied ~6 wt % O_3 in O_2 at 760 Torr. All the precursors were pulsed into the chamber using solenoid valves, and their flow was controlled using needle valves placed upstream. APTES was pulsed for 2 s followed by a 300-s Ar purge. H_2O was introduced into the chamber for 240 s followed by a 480-s purge step. A long Ar purge after H_2O exposure was required to ensure complete removal of any physisorbed H_2O on the cold walls of the reactor. O_3 was pulsed for 480 s followed by a 120-s Ar purge. The maximum chamber pressures during APTES, H_2O, and O_3 exposure were ~100, 30, and 80 mTorr, respectively. The chamber pressure during Ar purge was ~90 mTorr.

For ligand-exchange studies, the surface of the ZnSe IRC was prepared by coating it with SiO_2 through 10−15 ALD cycles at 150 °C, which consisted of APTES, H_2O, and O_3 in the sequence described above. Thus, the starting surface for APTES chemisorption is the same as that obtained after a complete ALD cycle. The temporal stability of the prepared surface was monitored and confirmed by recording IR spectra over a period of 1 h. An IR difference spectrum over the range of 4000−750 cm^{-1}, with a spectral resolution of ~4 cm^{-1}, was recorded after each precursor exposure cycle: all spectra are reported without baseline correction.

3. RESULTS AND DISCUSSION

Different surface species detected during each reaction cycle of APTES, H_2O, and O_3 at 150 °C are shown in the IR difference spectra in Figure 2. In these IR difference spectra, where a new background spectrum was collected before each reaction cycle, species freshly chemisorbed on the surface show an increase in IR absorbance while a decrease in IR absorbance can be interpreted as removal of those species or their reaction with the chemical moieties already present on the surface. Although not directly observed in spectra (a)−(c) in Figure 2, a one-to-one exchange of surface species can be interpreted from the IR difference spectra in the inset in Figure 2. Here, the reference spectrum for the oxidation cycle was collected after the APTES cycle, which

dx.doi.org/10.1021/cm103052t |*Chem. Mater.* 2011, 23, 2312–2316

means that it represents the *overall* ligand exchange during oxidation, and not for H_2O and O_3 cycles individually as in spectra (b) and (c), respectively, in Figure 2. An IR difference spectrum recorded after the APTES cycle is shown in Figure 2a. An increase in IR absorbance in the 3000−2800 cm^{-1} region was due to symmetric and asymmetric CH_x (x = 2, 3) stretching vibrations in the ethoxy and aminopropyl ligands of APTES.[26−30] The vibrational bands at 2981 and 2902 cm^{-1} correspond to the CH_3 asymmetric and symmetric stretching modes, respectively. Asymmetric and symmetric stretching bands of CH_2 appear at 2935 and 2865 cm^{-1}, respectively.[29,31,32] Since the peaks due to CH_3 and CH_2 stretching vibrations in ethoxy and aminopropyl ligands appear at very similar frequencies, it was difficult to distinguish the hydrocarbons in the two ligands.[26,28,29] In addition, NH_2 stretching modes (3400−3200 cm^{-1}),[26,29] NH_2 deformation modes (1600−1550 cm^{-1}),[26,29] CH_3 deformation modes (1400−1300 cm^{-1}),[26,30] Si−O−C stretching modes (1150−1050 cm^{-1}),[26,28] and NH_2 wagging modes (900−850 cm^{-1}) were observed in the IR spectrum in Figure 2a.[29] The band due to NH_2 stretching vibrations was broad due to intermolecular hydrogen bonding. A slight degree of polymerization of APTES on the surface due to the presence of a trace amount of H_2O may also cause broadening of the NH_2 stretching band. However, the chamber was purged with Ar for 480 s after every H_2O cycle to ensure the absence of any adventitious H_2O during the APTES cycle. A weak and broad mode at 1580 cm^{-1} was assigned to NH_2 deformation vibrations.[29,31] The weak IR bands at 1390 and 1300 cm^{-1} were assigned to CH_2 bending and wagging modes, respectively, in aminopropyl ligands.[26,30] The strong asymmetric and symmetric stretching modes of C−O in ethoxy ligands were centered at 1112 and 1083 cm^{-1}, respectively.[26,28,30] These bands in tetraethoxysilane have been reported at 1107 and 1083 cm^{-1}.[28] The shoulder at 1160 cm^{-1} was identified as the Si−O stretching vibration in $Si-OC_2H_5$.[26] This vibrational band has also been ascribed to the CH_3 rocking mode in ethoxy ligands of APTES.[30] Although the signal-to-noise ratio in the spectral region below 1000 cm^{-1} decreased dramatically, the shoulder at 960 cm^{-1} and a strong vibrational mode at 775 cm^{-1} could be distinguished and attributed to the CH_3 rocking mode[29,30] and the NH_2 wagging mode,[29,33] respectively, in the aminopropyl ligands. The NH_2 wagging mode at 775 cm^{-1} has been further confirmed by isotope exchange studies where a red shift of 145 cm^{-1} was observed for the ND_2 wagging mode.[29,33] Detailed identification of these peaks adequately confirms the chemisorption of APTES on the surface at 150 °C.

In addition to the increase in the above absorption features, there was a decrease in the IR absorbance in the 3800−3400, 2350−2250, and 1800−1650 cm^{-1} regions: the corresponding reactions that lead to these changes are discussed below. The decrease in IR absorbance in 3800−3400 cm^{-1} was due to the consumption of OH groups already present on the surface, suggesting that the ethoxy ligands of APTES react with the OH groups during chemisorption, releasing C_2H_5OH.[30] Self-catalytic hydrolysis of ethoxy ligands with surface OH groups or H_2O has been previously reported in the literature.[14,30] The broad nature of the absorbance in the 3800−3400 cm^{-1} region and the absence of a sharp peak at 3741 cm^{-1} due to isolated OH groups suggest hydrogen-bonded surface OH groups.[14] On the other hand, the decrease in IR absorbance centered at 1745 cm^{-1} has been attributed to C═O stretching vibration in crystalline formic acid where the OH group in each molecule is hydrogen-bonded to a carbonyl oxygen atom of a neighboring molecule.[34] The different hydrogen-bonding configurations that result in frequency shifts have been discussed by Mikawa et al.[34] The C═O stretching mode of molecularly physisorbed formic acid on SiO_2 appears at 1720 cm^{-1} due to the interaction of the carbonyl oxygen atom with a surface Si atom, which causes the observed frequency shift.[35−37] The C═O stretching vibration in the absence of any atomic interactions appears at ∼1770 cm^{-1} as in the case for gaseous formic acid.[38] The very weak negative absorption feature centered at 2277 cm^{-1} is attributed to Si−H stretching vibrations where the Si atom is backbonded to O atoms in SiO_2.[39] The specific origin of the species corresponding to the peaks at 2277 and 1749 cm^{-1} in our experiments will be discussed in detail later as we show that these species are actually formed after O_3 exposure.

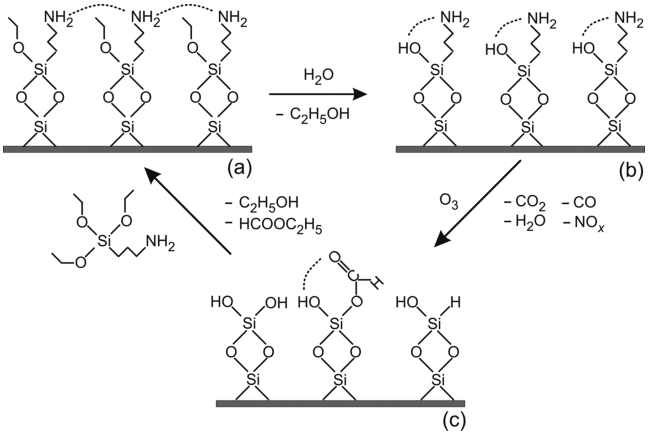

Figure 3. Schematic showing the surface reactions during ALD of SiO_2 from APTES, H_2O, and O_3. The dotted lines represent possible hydrogen-bonding configurations.

The IR difference spectrum recorded after the H_2O exposure cycle is shown in Figure 2b. The NH_2 groups in APTES most likely facilitate the self-catalytic hydrolysis of ethoxy ligands producing C_2H_5OH, which otherwise requires the presence of an acidic or basic catalyst.[17] The removal of ethoxy ligands can be inferred by observing the decrease in IR absorbance due to the strong C−O stretching modes at 1112 and 1083 cm^{-1}.[28,30] In addition, the decrease in absorbance in the 3000−2800 cm^{-1} region due to asymmetric and symmetric stretching modes of CH_3 and CH_2 further support the removal of the ethoxy ligands. An increase in IR absorption in the 3800−3400 cm^{-1} due to O−H stretching vibrations indicates that the hydrolysis of ethoxy ligands leaves the surface OH-terminated. The vibrational band in this region was very broad, suggesting hydrogen-bonded OH groups on the surface.[20,40] These OH groups can form hydrogen bonds with neighboring OH groups or NH_2 groups present in the aminopropyl ligands. The IR peak due to Si−OH when OH groups are hydrogen-bonded to an O atom of a neighboring OH group appears at 944 cm^{-1}.[40] Instead, a strong IR band at ∼1000 cm^{-1} was observed and has been assigned to Si−OH where OH groups were hydrogen-bonded to an N atom of a neighboring NH_2 group (see Figure 2b).[27] Thus, the hydrolyzed surface was terminated with OH groups along with aminopropyl ligands where OH groups were hydrogen-bonded to NH_2 groups, as shown in Figure 3.

An IR difference spectrum recorded after the O_3 cycle is shown in Figure 2c. The removal of aminopropyl ligands upon

O_3 exposure was corroborated by the decrease in IR absorbance in the 3400−3200 cm^{-1} (broad and very weak),[29] 3000−2800 cm^{-1} (strong),[26,29,30] 1150−1050 cm^{-1} (strong),[29] 900−850 cm^{-1} (medium),[29] and 800−750 cm^{-1} (strong) regions:[29] these spectral regions correspond to NH_2 stretching,[29] CH_3 and CH_2 stretching,[26,29,30] C−N stretching (∼1097 cm^{-1}),[29] C−C−C stretching (876 cm^{-1}),[29] and NH_2 wagging (775 cm^{-1}) modes, respectively, in the aminopropyl ligands.[29] The Si−OH species, where the OH groups were hydrogen-bonded to NH_2 groups, were also removed as concluded from the decrease in the IR vibrational mode at ∼1000 cm^{-1}. In addition, an increase in IR absorbance at 2277, 1745, and 1220 cm^{-1} was observed. As discussed earlier, the IR band at 1745 cm^{-1} can be assigned to the C═O stretching mode in crystalline hydrogen-bonded formic acid. However, the possibility of gaseous and crystalline formic acid can be eliminated as the spectrum in Figure 2c was collected after evacuating all the reaction products from the chamber. It is also very unlikely that formic acid is physisorbed on SiO_2 at the temperature of the experiment because it readily desorbs at 378 K from a SiO_2 surface.[41] Huang et al. and Tanaka et al. have reported that dissociative adsorption of formic acid onto a pristine Si(111) surface produces a monodentate formate [Si−O−C(H)═O] with an H atom transferred to an adjacent Si atom.[36,37] A monodentate formate on Si maintains a C═O character as shown in Figure 3. Different authors have previously reported the formation of formates[42] and carbonates[18,19] during ALD of metal oxides when O_3 was used as an oxidizer. From previous studies, we know that O_3 combusts the hydrocarbon ligands, in this case aminopropyl, producing most likely CO, CO_2, H_2O, and NO_x.[18,19] According to the catalysis literature, formates are formed due to the reaction of CO with OH groups on the surface, which were present after the H_2O cycle.[43] Thus, a monodentate formate is likely to be formed on the surface after O_3 exposure. Therefore, we assign the IR vibrational bands at 1745 and 1220 cm^{-1} to C═O stretching and C−O stretching modes in monodentate formate on SiO_2.[36,37] The carbonyl oxygen atoms in these formates are hydrogen-bonded to H atoms of neighboring OH groups, causing the frequency to shift from 1770 cm^{-1} (interaction free C═O) to 1745 cm^{-1} (hydrogen-bonded C═O).[34,38] The band at 2277 cm^{-1} is assigned to SiH stretching in O_3Si-H, which may be formed due to dissociative adsorption of formic acid producing an H atom on an adjacent Si atom.[39] Both monodentate formate and SiH species were stable at 150 °C.

On the basis of the IR data in Figure 2, a schematic view of the complete reaction mechanism during ALD of SiO_2 is shown in Figure 3. Figure 3a shows APTES chemisorbed on the SiO_2 surface. When this surface is exposed to H_2O at 150 °C, a self-catalytic hydrolysis reaction of ethoxy ligands produces C_2H_5OH, which is evacuated from the chamber. This hydrolysis reaction leaves the surface OH-terminated along with aminopropyl ligands. Depending on the spatial configuration of the chemisorbed species, H in OH groups may be hydrogen-bonded to NH_2 groups on the same site or a neighboring site. This OH-terminated surface in Figure 3b is then exposed to O_3, which combusts the aminopropyl groups, producing CO, CO_2, H_2O, and NO_x. Among these volatile products, CO reacts with the surface OH groups, producing monodentate formates and SiH. Some OH groups are also produced due to H_2O produced in the reaction. When the surface in Figure 3c is exposed to APTES, it reacts with the OH groups and SiH, producing primarily ethanol (Figure 3a). We speculate that the reaction of APTES with monodentate formates on the surface may produce a stable compound, ethyl formate, thus regenerating the surface in Figure 3a, which is necessary for an ALD process.

4. CONCLUSIONS

Different surface species during ALD of SiO_2 from APTES, H_2O, and O_3 were detected using in situ ATR-FTIR spectroscopy. Use of APTES offers advantages over the more conventional SiO_2 precursor, tetraethoxysilane, by avoiding the requirement of a catalyst to hydrolyze the ethoxy ligands to produce ethanol. Although the use of O_3 to combust the remaining aminopropyl ligands after hydrolysis of APTES produced monodentate formates and SiH on the surface, these species were reactive to APTES chemisorption, thus providing a suitable pathway to deposit relatively contamination-free SiO_2 films. A detailed future study using a quartz crystal microbalance would be needed to calculate the number of ligands exchanged during each half reaction cycle, the number of available surface sites, and the growth rate.

■ ASSOCIATED CONTENT

Ⓢ Supporting Information. IR difference spectrum recorded after the O_3 cycle, showing the asymmetric and symmetric Si−O−Si stretching vibrations in SiO_2 at 150 °C. The spectral region in 1300−950 cm^{-1} was fitted with 4 Gaussian bands centered at 1056, 1160, 1200, and 1245 cm^{-1}. This material is available free of charge via the Internet at http://pubs.acs.org.

■ AUTHOR INFORMATION

Corresponding Author

*To whom correspondence should be addressed. E-mail: sagarwal@mines.edu.

■ ACKNOWLEDGMENT

We gratefully acknowledge support from the NSF CAREER program (Grant No. CBET-0846923), the NSF Renewable Energy MRSEC program at the Colorado School of Mines (Grant No. DMR-0820518), and the Center for Revolutionary Solar Photoconversion (Task No. KXFE-9-99001-08).

■ REFERENCES

(1) Robertson, J. *Rep. Prog. Phys.* **2006**, *69*, 327.
(2) Methaapanon, R.; Bent, S. F. *J. Phys. Chem. C* **2010**, *114*, 10498.
(3) Ho, M. T.; Wang, Y.; Brewer, R. T.; Wielunski, L. S.; Chabal, Y. J.; Moumen, N.; Boleslawski, M. *Appl. Phys. Lett.* **2005**, *87*, 133103.
(4) George, S. M.; Ott, A. W.; Klaus, J. W. *J. Phys. Chem.* **1996**, *100*, 13121.
(5) Puurunen, R. L. *J. Appl. Phys.* **2005**, *97*, 52.
(6) Zhong, L. J.; Chen, F.; Campbell, S. A.; Gladfelter, W. L. *Chem. Mater.* **2004**, *16*, 1098.
(7) Rowlette, P. C.; Wolden, C. A. *ACS Appl. Mater. Interfaces* **2009**, *1*, 2586.
(8) Lee, J. Y.; Glunz, S. W. *Sol. Energy Mater. Sol. Cells* **2006**, *90*, 82.
(9) Waggoner, P. S.; Tan, C. P.; Craighead, H. G. *J. Appl. Phys.* **2010**, *107*, 114505.
(10) Ferguson, J. D.; Weimer, A. W.; George, S. M. *Chem. Mater.* **2000**, *12*, 3472.
(11) Lee, J. H.; Kim, U. J.; Han, C. H.; Rha, S. K.; Lee, W. J.; Park, C. O. *Jpn. J. Appl. Phys.* **2004**, *43*, L328.

(12) Lim, J. W.; Yun, S. J.; Lee, J. H. *ETRI J.* **2005**, *27*, 118.
(13) Gasser, W.; Uchida, Y.; Matsumura, M. *Thin Solid Films* **1994**, *250*, 213.
(14) Ferguson, J. D.; Smith, E. R.; Weimer, A. W.; George, S. M. *J. Electrochem. Soc.* **2004**, *151*, G528.
(15) Miller, K. A.; John, C.; Zhang, K. Z.; Nicholson, K. T.; McFeely, F. R.; Holl, M. M. B. *Thin Solid Films* **2001**, *397*, 78.
(16) Burton, B. B.; Boleslawski, M. P.; Desombre, A. T.; George, S. M. *Chem. Mater.* **2008**, *20*, 7031.
(17) Bachmann, J.; Zierold, R.; Chong, Y. T.; Hauert, R.; Sturm, C.; Schmidt-Grund, R.; Rheinlander, B.; Grundmann, M.; Gosele, U.; Nielsch, K. *Angew. Chem.-Int. Ed.* **2008**, *47*, 6177.
(18) Rai, V. R.; Vandalon, V.; Agarwal, S. *Langmuir* **2010**, *26*, 13732.
(19) Rai, V. R.; Agarwal, S. *J. Phys. Chem. C* **2008**, *112*, 9552.
(20) Rai, V. R.; Agarwal, S. *J. Phys. Chem. C* **2009**, *113*, 12962.
(21) Agarwal, S.; Sriraman, S.; Takano, A.; van de Sanden, M. C. M.; Aydil, E. S.; Maroudas, D. *Surf. Sci.* **2002**, *515*, L469.
(22) Agarwal, S.; Valipa, M. S.; Hoex, B.; van de Sanden, M. C. M.; Maroudas, D.; Aydil, E. S. *Surf. Sci.* **2005**, *598*, 35.
(23) Chabal, Y. J. *Surf. Sci. Rep.* **1988**, *8*, 211.
(24) Agarwal, S.; Takano, A.; van de Sanden, M. C. M.; Maroudas, D.; Aydil, E. S. *J. Chem. Phys.* **2002**, *117*, 10805.
(25) Agarwal, S.; Hoex, B.; van de Sanden, M. C. M.; Maroudas, D.; Aydil, E. S. *J. Vac. Sci. Technol. B* **2004**, *22*, 2719.
(26) Buining, P. A.; Humbel, B. M.; Philipse, A. P.; Verkleij, A. J. *Langmuir* **1997**, *13*, 3921.
(27) White, L. D.; Tripp, C. P. *J. Colloid Interface Sci.* **2000**, *232*, 400.
(28) Deshmukh, S. C.; Aydil, E. S. *J. Vac. Sci. Technol. A* **1995**, *13*, 2355.
(29) Durig, J. R.; Beshir, W. B.; Godbey, S. E.; Hizer, T. J. *J. Raman Spectrosc.* **1989**, *20*, 311.
(30) Pena-Alonso, R.; Rubio, F.; Rubio, J.; Oteo, J. L. *J. Mater. Sci.* **2007**, *42*, 595.
(31) Pasternack, R. M.; Amy, S. R.; Chabal, Y. J. *Langmuir* **2008**, *24*, 12963.
(32) Tedder, L. L.; Lu, G. Q.; Crowell, J. E. *J. Appl. Phys.* **1991**, *69*, 7037.
(33) Sato, N.; Hamada, Y.; Tsuboi, M. *Spectrochim. Acta, Part A* **1987**, *43*, 943.
(34) Mikawa, Y.; Brasch, J. W.; Jakobsen, R. J. *J. Mol. Spectrosc.* **1967**, *24*, 314.
(35) Chen, M. T.; Lin, Y. S.; Lin, Y. F.; Lin, H. P.; Lin, J. L. *J. Catal.* **2004**, *228*, 259.
(36) Huang, J. Y.; Huang, H. G.; Lin, K. Y.; Liu, Q. P.; Sun, Y. M.; Xu, G. Q. *Surf. Sci.* **2004**, *549*, 255.
(37) Tanaka, S.; Onchi, M.; Nishijima, M. *J. Chem. Phys.* **1989**, *91*, 2712.
(38) Cabilla, G. C.; Bonivardi, A. L.; Baltanas, M. A. *Appl. Catal., A* **2003**, *255*, 181.
(39) Gupta, P.; Dillon, A. C.; Bracker, A. S.; George, S. M. *Surf. Sci.* **1991**, *245*, 360.
(40) Davis, K. M.; Tomozawa, M. *J. Non-Cryst. Solids* **1996**, *201*, 177.
(41) Li, G. X.; Ridd, M. J.; Larkins, F. P. *Aust. J. Chem.* **1991**, *44*, 623.
(42) Goldstein, D. N.; McCormick, J. A.; George, S. M. *J. Phys. Chem. C* **2008**, *112*, 19530.
(43) Busca, G.; Lorenzelli, V. *Mater. Chem.* **1982**, *7*, 89.